IEEE Access
Multidisciplinary | Rapid Review | Open Access Journal

Received November 25, 2019, accepted December 3, 2019, date of publication December 10, 2019,
date of current version December 23, 2019.

Digital Object Identifier 10.1109/ACCESS.2019.2958569

Adaptive Neural Network Nonsingular Fast Terminal Sliding Mode Control for Permanent Magnet Linear Synchronous Motor

XIMEI ZHAO AND DONGXUE FU
School of Electrical Engineering, Shenyang University of Technology, Shenyang 110870, China
Corresponding author: Ximei Zhao (zhaoxm_sut@163.com)

This work was supported by the Liaoning Provincial Natural Science Foundation of China under Grant 20170540677.

ABSTRACT For the problem that the position tracking accuracy of permanent magnet linear synchronous motor (PMLSM) servo system is easily affected by uncertain factors such as parameters change, load disturbance and friction and so on, an adaptive neural network nonsingular fast terminal sliding mode control (ANNNFTSMC) method is proposed. Firstly, the PMLSM dynamic mathematical model with uncertainty is established. Then, the nonsingular fast terminal sliding mode control (NFTSMC) can avoid the singularity problem and make the state of the system converge to the equilibrium point quickly, so as to improve the response speed of the system. Secondly, in order to minimize the influence of disturbance and dynamic uncertainty, the dynamic model of PMLSM servo system is estimated by RBF neural network, and the uncertain upper bound of PMLSM servo system is estimated in real time combined with adaptive control, which weakens the chattering phenomenon and enhances the robustness of the system. It is proved theoretically that the control scheme can make the system achieve fast convergence and good tracking. Finally, the system experiments show that the proposed control scheme has the advantages of high tracking accuracy, good robustness, fast response speed and small position error.

INDEX TERMS Permanent magnet linear synchronous motor, nonsingular fast terminal sliding mode control, adaptive, RBF neural network.

I. INTRODUCTION

Permanent Magnet Linear Synchronous Motor (PMLSM) is an important core component of automation equipment such as robot equipment, computer numerical control, XY platform [1]. The control performance of PMLSM directly affects the performance of the device, so improving the dynamic tracking performance of PMLSM has always been the focus of research in this field. However, PMLSM is a nonlinear and uncertain object. It is difficult to obtain accurate mathematical models in practice, and PMLSM adopts direct drive structure, which reduces the elastic deformation between traditional mechanical structures and improves the stiffness of the transmission system [2]. The reduction of the intermediate buffer mechanism causes many uncertain factors to directly act on the PMLSM mover, which poses a severe challenge to achieve system control and improve performance. Therefore, it is necessary to design a strong robust controller to suppress these uncertainties and improve the control performance of the system [3].

Traditional control methods usually do not require accurate dynamic models, but in the presence of disturbances and dynamic uncertainties, these traditional control methods do not achieve the desired control performance. In order to improve the control performance of the system, several advanced control methods have been proposed, such as fuzzy control [4]–[6], neural network control [7]–[9], adaptive control [10]–[12] and sliding mode control [13]–[15], etc., but the effectiveness of each method has certain limitations. Among these control methods, SMC is robust to the uncertainties and disturbances of nonlinear systems, so SMC has been widely used. However, traditional SMC still has defects, such as the need for accurate dynamic models, singularity problems, chattering phenomena, and finite time convergence. In order to solve these shortcomings, relevant scholars at home and abroad have conducted research and achieved some results.

The associate editor coordinating the review of this manuscript and approving it for publication was Bo Shen.

In [16], the integral sliding mode surface is used to improve the control precision of the system, but the calculation is more complicated and the system state convergence speed is slower. In [3], adaptive incremental sliding mode control is utilized. Based on SMC, the previous state and control actions of the system are used as feedback quantities. At the same time, adaptive control is used to estimate the total uncertainty of the system in real time, but the system is too dependent on the previous state, and when there is a particularly large external disturbance, it is easy to cause the system to crash. In [17], the modular controller is designed by using the fast terminal sliding mode control method, which improves the system convergence speed and reduces the chattering. However, when the system is in a specific subspace of the state space, the controller's output signal will appear infinite. In [18], adaptive nonsingular terminal sliding mode control method is adopted. Adaptive control is used to estimate the upper bound of system uncertainty and convert the discontinuous signal function into the time derivative of the control input. After integration, the continuous control signal is obtained. Under the premise of not affecting the robustness of the system, the chattering phenomenon is improved, but the convergence speed of the system is still relatively slow. In [19], a backstepping control method based on adaptively modified Laguerre recurrent neural network is proposed. Although the two optimal learning rates are derived to accelerate the parameter convergence to a certain extent, the Laguerre neural network is computationally complex. The problem of degree is still not well resolved. In [20], the radial basis function neural network is used to approximate the uncertain function in the system, and combined with the inverse method to make the system robust to interference, but the convergence speed of the system state variable is slow. In [21], a nonsingular fast terminal sliding mode control (NFTSMC) method is proposed to avoid the singularity problem and ensure that the system tracking error converges to zero in a finite time, which improves the tracking of the system, but when the system appears larger uncertain disturbances can cause the system to become unstable. In [22], a fast nonsingular integral terminal sliding mode and adaptive control technology are combined to propose an adaptive fast nonsingular integral terminal sliding mode control (AFNITSM) method. The control method improves the convergence speed of the trajectory tracking control of the autonomous underwater vehicles (AUVs), so that the speed and position tracking errors converge to zero within a finite time. However, when more complex orbits and greater environmental disturbances occur, the tracking performance and robustness of the system will deteriorate. In [23], In order to solve the trajectory tracking problem of fully actuated autonomous underwater vehicles with dynamic uncertainty and time-varying external disturbance, an adaptive second-order fast nonsingular terminal sliding mode control scheme is proposed. Using adaptive to estimate the unknown parameters of uncertainty in the system, and introducing a discontinuous symbol function in the control input, the chattering phenomenon is weakened without reducing the tracking accuracy, and the trajectory tracking control has a faster convergence speed. However, the convergence speed of the system is still relatively slow. In [24]–[26], the design method combining time-delay control and terminal sliding mode control is adopted. The time-delay estimation (TDE) technique is applied to cancel out complicated nonlinear dynamics guaranteeing an excellent model-free scheme. The terminal sliding mode control ensures fast dynamic response at the reaching stage, enabling the system to achieve higher convergence speed and tracking accuracy. However, when a particularly large disturbance occurs in the system, the robustness of the system may be difficult to guarantee.

In this paper, an adaptive neural network nonsingular fast terminal sliding mode control (ANNNFTSMC) method is designed. First, the adaptive control is combined with the RBF neural network to approximate the unknown part function of the PMLSM and estimate the upper bound of the system uncertainty, eliminating the need for accurate dynamic models and improving the tracking accuracy of the system. On this basis, the use of NFTSMC can eliminate singularity problems and improve the system's response speed. The main advantages of this control method include:

1) The ANNNFTSMC method inherits the advantages of nonsingularity, finite time convergence, fast transient response, low steady-state error and high tracking accuracy.
2) The achievement of smooth control inputs with chattering behavior elimination.
3) The removal of demand for an exact dynamic model by applying an adaptive radial basis function neural network to approximate an unknown PMLSM function.
4) Better tracking performance and less impact by disturbances and uncertainties compared to NFTSMC.

In summary, the experimental results show that the proposed method can weaken the chattering and improve the tracking performance and robust performance of the system.

The structure of this paper is dealt with as follows: Section 2 introduces the basic structure and mathematical model of PMLSM. Section 3 demonstrates the design of NFTSMC and ANNNFTSMC through Lyapunov stability analysis. Section 4 introduces the system experiment and performs a verification analysis. Finally, Section 5 concludes the paper.

II. BASIC STRUCTURE AND MATHEMATICAL MODEL OF PMLSM

In this part, the main introduction to the basic structure, basic working principle and mathematical model of PMLSM.

A. THE BASIC STRUCTURE OF PMLSM

The PMLSM is mounted on the stator side in a straight line along the full stroke direction, and N and S pole permanent magnets are alternately mounted one after another, as shown in Fig. 1. On the whole length below the mover, the energized winding containing the iron core is correspondingly installed (the permanent magnet synchronous rotating

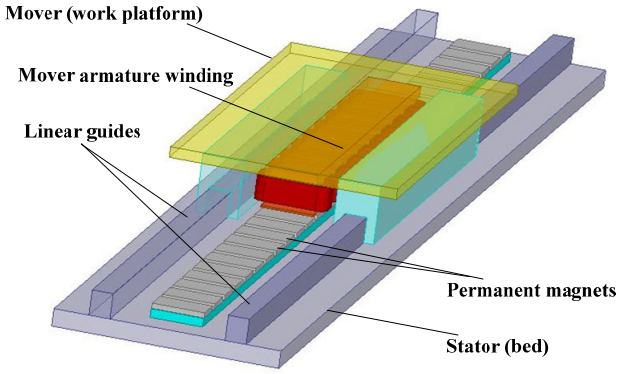

FIGURE 1. Schematic diagram of the PMLSM structure.

electric machine is a permanent magnet mounted on the rotor, and the armature winding is included in the stator). To do this, the mover must be moved with the cable, and its top view is shown in Fig. 2.

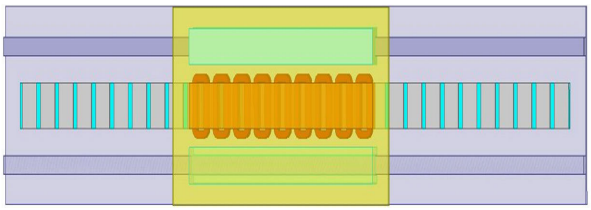

FIGURE 2. Top view of the PMLSM.

B. BASIC WORKING PRINCIPLE OF PMLSM

The linear motor is not only similar in structure to the rotating motor, but also works similarly. Fig. 3 shows a schematic diagram of the working principle of a PMLSM. After a three-phase symmetrical sinusoidal current is applied to the three-phase winding of the linear motor mover, an air gap magnetic field is also generated. When the longitudinal end effect due to the breaking of the two ends of the core is not considered, the distribution of the air gap magnetic field is similar to that of the rotating electric motor, that is, it can be regarded as a sinusoidal distribution along the linear direction of the

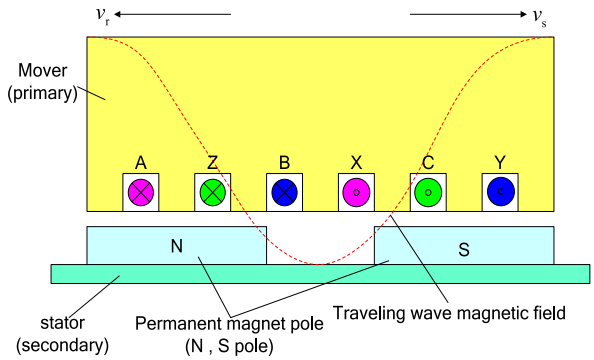

FIGURE 3. Schematic diagram of PMLSM working principle.

unfolding. When the three-phase current changes with time, the air gap magnetic field will move in a straight line in the A, B, C phase sequence. This principle is similar to a rotating motor, but the difference between the two is that the air gap magnetic field of the linear motor is translated in a linear direction rather than rotated. Therefore, this magnetic field is called a traveling wave magnetic field. Obviously, the moving speed of the traveling wave magnetic field is the same as the linear velocity v_s (referred to as the synchronous speed) of the rotating magnetic field on the inner circular surface of the stator. For PMLSM, the excitation field of the permanent magnet interacts with the traveling wave magnetic field to generate electromagnetic thrust. Under the action of electromagnetic thrust, since the stator is fixed, the mover (i.e., the primary) will move linearly in the opposite direction of the traveling wave magnetic field, and its velocity is v_r. The above is the basic working principle of PMLSM.

C. MATHEMATICAL MODEL OF PMLSM

In this paper, surface-mount PMLSM is used, in which PMLSM adopts d-q axis current control, and q-axis leads d-axis 90° electrical angle. Since the motor is a nonlinear time-varying controlled object, it is difficult to accurately model. In the process of modeling, the corresponding assumptions and neglects were made to abstract the motor into an "ideal motor" for model building. Now assume:

1) Ignore the saturation of the core;
2) Excluding eddy current and hysteresis loss;
3) There is no damper winding on the primary, and the permanent magnet has no damping effect;
4) The back electromotive force is sinusoidal.

Since only the fundamental component of each variable is considered, the d-q axis model can be used [27]. Since the magnetomotive force generated by the permanent magnet is constant and there is no damper winding on the secondary, assuming that its equivalent inductance is L_f and the equivalent excitation current is i_f, the d-q axis model flux linkage equation of PMLSM is

$$\psi_d = L_d i_d + L_f i_f \tag{1}$$
$$\psi_q = L_q i_q \tag{2}$$
$$\psi_f = L_f i_f \tag{3}$$

where ψ_d, ψ_q, i_d, i_q, L_d, and L_q are the flux, current, and inductance of the d and q axes, respectively; ψ_f, L_f and i_f are the fundamental flux linkage, equivalent inductance and equivalent current generated by the permanent magnet respectively.

The voltage equation of the d-q axis model of PMLSM is

$$u_d = R_s i_d + \frac{d\psi_d}{dt} - \omega\psi_q \tag{4}$$
$$u_q = R_s i_q + \frac{d\psi_q}{dt} + \omega\psi_q \tag{5}$$

where u_d and u_q are the d and q axis voltages of the mover, R_s is the stator resistance, $\omega = v\pi/\tau$ is the electrical angular

velocity, v is the velocity of the mover, and τ is the polar moment.

The electromagnetic thrust equation of PMLSM is

$$F_{\mathrm{e}} = \frac{3\pi n_{\mathrm{p}}}{2\tau}\left[\psi_{\mathrm{PM}} - \left(L_{\mathrm{q}} - L_{\mathrm{d}}\right) i_{\mathrm{d}}\right] i_{\mathrm{q}} \tag{6}$$

where p_{n} is the pole logarithm. Since the PMLSM air gap is large, the salient pole effect of the magnetic pole is negligible, so the direct-axis excitation inductance is approximately equal to the cross-axis excitation inductance $L_{\mathrm{d}} = L_{\mathrm{q}}$, so the electromagnetic thrust can be simplified to

$$F_e = \frac{3\pi n_{\mathrm{p}}}{2\tau}\psi_{\mathrm{PM}} i_{\mathrm{q}} = K_{\mathrm{f}} i_{\mathrm{q}} \tag{7}$$

$$K_{\mathrm{f}} = \frac{3\pi n_{\mathrm{p}}}{2\tau}\psi_{\mathrm{PM}} \tag{8}$$

where K_{f} is the electromagnetic thrust constant.

The mechanical equation of motion of PMLSM is

$$F_e = M\dot{v} + Bv + F \tag{9}$$

where M is the total mass of the mover of PMLSM; V is the velocity of the mover; B is the viscous friction coefficient; F is the nonlinear disturbance, and F includes the external disturbance of the system, the nonlinear friction and the change of the system parameters.

When the disturbance F is not considered, the dynamic equation is

$$\ddot{d}(t) = -\frac{B}{M}\dot{d}(t) + \frac{K_{\mathrm{f}}}{M} i_{\mathrm{q}} = A_{\mathrm{n}}\dot{d}(t) + B_{\mathrm{n}} u \tag{10}$$

where $d(t)$ is the position of the mover, $A_{\mathrm{n}} = -B/M$; $B_{\mathrm{n}} = K_{\mathrm{f}}/M$; u is the output of the controller; $u = i_{\mathrm{q}}$, i.e., the thrust current.

When considering disturbances, the dynamic equation is

$$\begin{aligned}\ddot{d}(t) &= (A_{\mathrm{n}} + \Delta A)\,\dot{d}(t) + (B_{\mathrm{n}} + \Delta B)\,u + (C_{\mathrm{n}} + \Delta C)\,F \\ &= A_{\mathrm{n}}\dot{d}(t) + B_{\mathrm{n}} u + D\end{aligned} \tag{11}$$

where $C_{\mathrm{n}} = -1/M$; ΔA, ΔB, and ΔC are the uncertainties caused by the system parameters M and B, respectively;

$$D = \Delta A\dot{d}(t) + \Delta B u + (C_{\mathrm{n}} + \Delta C)\,F \tag{12}$$

Here, suppose D is bounded, that is, $|D| \le \delta$, δ is the upper bound of the uncertainty sum D, which is a positive constant.

III. DESIGN PROCEDURE FOR A CONTROL STRATEGY

A block diagram of the PMLSM servo system based on ANNNFTSMC is shown in Fig. 4. In Fig. 4, ANNNFTSMC is designed based on the combination of adaptive control and RBF neural network based on NFTSMC. NFTSMC realizes that the system reaches the sliding surface in a limited time, and makes the position tracking error close to zero in a limited time, which improves the rapidity of the system state; the RBF neural network is used to approximate the unknown function in PMLSM to obtain an accurate PMLSM dynamic model; Adaptive control is used to estimate the upper bound of uncertainty in neural network in real time and further improve the robustness of the system.

A. DESIGN OF NONSINGULAR FAST TERMINAL SLIDING MODE CONTROLLERS

Based on the terminal sliding mode design method, the NFTSMC method is designed. The NFTSMC method is proposed according to the tracking position error.

Nonsingular fast terminal sliding surface is

$$S = \dot{\varsigma} + h_1 \mathrm{sign}\left(\varsigma\right) + h_2 \varsigma^{\alpha} \tag{13}$$

where h_1 and h_2 are positive constants and $\alpha > 1$.

The sliding surface variable ς is defined as

$$\varsigma = e + \int_0^t \left(\Gamma_1 e^{2-\theta} + \Gamma_2 e + \Gamma_3 e^{\theta}\right)\mathrm{d}\sigma \tag{14}$$

$$e^{\theta} = \mathrm{sig}(e)^{\theta} \tag{15}$$

where $e = d - d_{\mathrm{m}}$ is the tracking position error, d_{m} is the reference position input signal, d is the actual position output signal, $0 < \theta < 1$. Once the tracking error $|e|$ is much greater than 1, $\Gamma_1 e^{2-\theta} + \Gamma_2 e$ can cause the system to converge quickly. When $|e|$ tracking error is much less than 1, $\Gamma_3 e^{\theta}$ causes the system to converge for a limited time.

Substituting equation (14) into equation (13)

$$S = \dot{e} + \Gamma_1 e^{2-\theta} + \Gamma_2 e + \Gamma_3 e^{\theta} + h_1 \mathrm{sign}\left(\varsigma\right) + h_2 \varsigma^{\alpha} \tag{16}$$

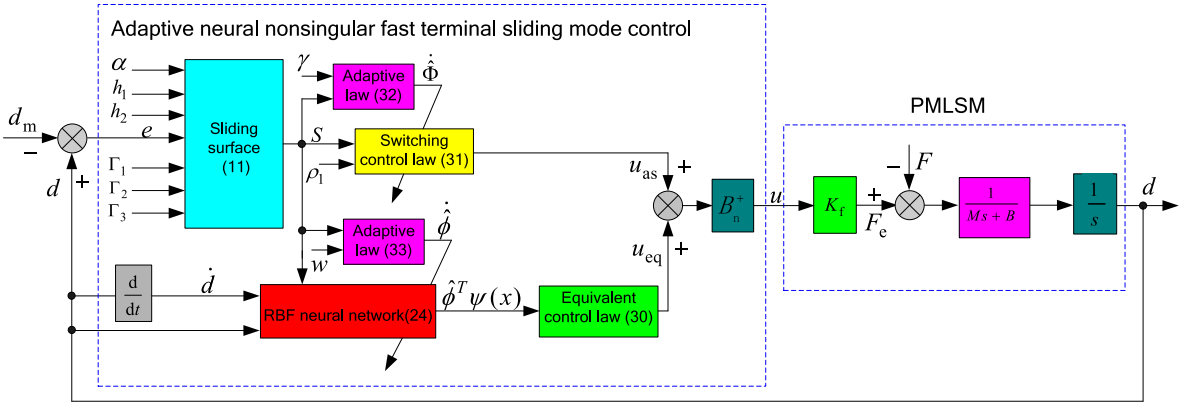

FIGURE 4. Block diagram of PMLSM servo control system based on ANNNFTSMC.

To simplify the analysis, apply the following concepts

$$\frac{\mathrm{d}e^{\theta}}{\mathrm{d}t} = \theta\,|e|^{\theta-1}\,\dot{e} \tag{17}$$

Combining equation (17)

$$\dot{S} = \ddot{e} + \Gamma_1\,(2-\theta)\,|e|^{1-\theta}\,\dot{e} + \Gamma_2\dot{e} + \Gamma_3\theta\,|e|^{\theta-1}\,\dot{e} + h_2\alpha\,|\varsigma|^{\alpha-1}\,\dot{\varsigma} \tag{18}$$

Known by equation (11), $\ddot{e}$ can be expressed as

$$\begin{aligned}\ddot{e} &= \ddot{d} - \ddot{d}_{\mathrm{m}} \\ &= -A_{\mathrm{n}}\dot{d} + B_{\mathrm{n}}u + D - \ddot{d}_{\mathrm{m}}\end{aligned} \tag{19}$$

Substituting equation (19) into equation (18)

$$\dot{S} = -A_{\mathrm{n}}\dot{d} + B_{\mathrm{n}}u + D - \ddot{d}_{\mathrm{m}} + \Pi\,(e,\varsigma) \tag{20}$$

$$\Pi\,(e,\varsigma) = \Gamma_1\,(2-\theta)\,|e|^{1-\theta}\,\dot{e} + \Gamma_2\dot{e} + \Gamma_3\theta\,|e|^{\theta-1}\,\dot{e} + h_2\alpha\,|\varsigma|^{\alpha-1}\,\dot{\varsigma} \tag{21}$$

In order to obtain the control performance required by the system, the overall control law is designed as

$$u = B_{\mathrm{n}}^{+}\left(u_{\mathrm{eq}} + u_{\mathrm{s}}\right) \tag{22}$$

where $B_{\mathrm{n}}^{+} = B_{\mathrm{n}}^{T}\left(B_{\mathrm{n}}B_{\mathrm{n}}^{T}\right)^{-1}$.

The equivalent control law is

$$u_{\mathrm{eq}} = A_{\mathrm{n}}\dot{d} - \Pi\,(e,\varsigma) + \ddot{d}_{\mathrm{m}} \tag{23}$$

Switching control law is

$$u_{\mathrm{s}} = -\,(\Omega + \rho_1)\,\mathrm{sign}\,(S) \tag{24}$$

where Ω and ρ_1 are positive constants.

Substituting equations (22), (23), and (24) into equation (20)

$$\dot{S} = -\,(\Omega + \rho_1)\,\mathrm{sign}\,(S) + D \tag{25}$$

Constructing Lyapunov function

$$V_1 = \frac{1}{2}S^2 \tag{26}$$

Combining equation (25), the time derivative of V_1 is derived as

$$\begin{aligned}\dot{V}_1 &= S\dot{S} \\ &= S\,(-\,(\Omega + \rho_1)\,\mathrm{sign}\,(S) + D) \\ &= -\Omega\,|S| - \rho_1\,|S| + DS \le -\rho_1\,|S|\end{aligned} \tag{27}$$

Therefore, in the case of external disturbances and system uncertainties, the stability of the system can still be guaranteed by Lyapunov's theorem.

B. DESCRIPTION OF NEURAL NETWORK MODEL

In this paper, RBF neural network is selected because of its good generalization ability, simple network structure, easy design, strong online learning ability and the ability to avoid unnecessary and lengthy calculations. The working principle of RBF neural network: From the point of view of function approximation, if the network is regarded as an approximation to an unknown function, any function can be expressed as a weighted sum of a set of basis functions. In the RBF network, it is equivalent to selecting the transfer function of each hidden layer neuron to form a set of basis functions to approximate the unknown function.

Research on RBF neural networks shows that RBF neural networks can approximate any nonlinear function in a compact set and arbitrary precision. Compared with BP neural networks, RBF neural networks are simpler and have faster convergence. The RBF neural network consists of three layers: the input layer, the hidden layer and the output layer, all of which are represented in Fig. 5.

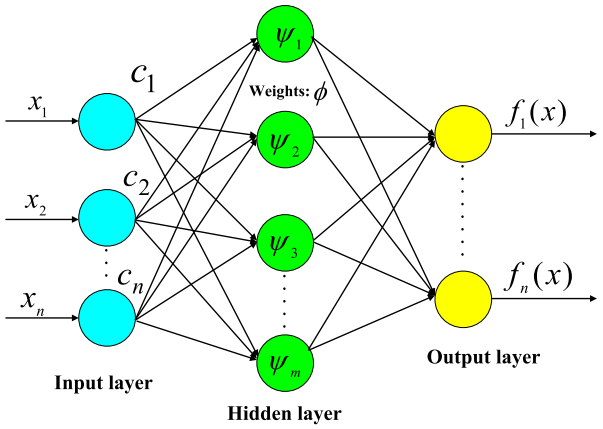

FIGURE 5. Structure of the RBF neural network.

RBF neural network output is

$$f(x) = \phi^{T}\psi(x) + \xi(x) \tag{28}$$

where $x \in \mathbb{R}^{\mathrm{n}}$ and $f(x)$ are the input and output of the neural network, $\phi^{T} \in \mathbb{R}^{\mathrm{n}\times\mathrm{m}}$ is the weight matrix connecting the hidden layer and the output layer, $\psi(x)$ is the nonlinear function of the hidden layer node, and $\xi(x) \in \mathbb{R}^{\mathrm{n}}$ is the approximate error of the neural network.

The nonlinear function of the hidden layer is represented by Gaussian function

$$\psi(x) = \exp\left(-\frac{\|x - c_i\|^2}{2b_i^2}\right) \quad i = 1, 2, \cdots, m \tag{29}$$

where b_i and c_i are the width and center of the Gaussian function, respectively.

C. DESIGN OF ADAPTIVE NEURAL NETWORK NONSINGULAR FAST TERMINAL SLIDING MODE CONTROLLERS

PMLSM has complex dynamic models and there are many parameter uncertainty problems (such as friction, disturbances, etc.). For this reason, it is very important to accurately calculate the upper bound of uncertainty and provide an accurate PMLSM dynamic function in the equivalent control law. In order to overcome these difficulties, an ANNNFTSMC method is proposed to control the PMLSM servo system. The adaptive RBF neural network is used to approximate the unknown dynamic function in PMLSM, and the adaptive law is used to estimate the upper bound of the system uncertainty.

RBF neural network is used to approximate the PMLSM model

$$f(x) = -A_{\mathrm{n}}\dot{d} \tag{30}$$

where $x = [\,x_1 \;\; x_2\,]^T$ and $x_1 = d, x_2 = \dot{d}$.

Define $\hat{f}(x)$ as an approximation of $f(x)$, which can be represented by a neural network as

$$\hat{f}(x) = \hat{\phi}^T\psi(x) \tag{31}$$

The optimal parameter ϕ^* is expressed as

$$\phi_H^* = \arg\min\left\{\sup_{x\in\Theta_x}\left|f(x) - \hat{f}(x,\hat{\phi})\right|\right\} \tag{32}$$

To better illustrate the problem, the cited lemma is as follows:

Lemma [28]: For a given real continuous function $f(X)$, when set $\Theta_X \in R^{\mathrm{n}}$ and any positive coefficient $\xi > 0$, there will be a neural network approximator $\hat{f}(X)$

$$\sup_{X\in\Theta_X}\left|f(X) - \hat{f}(X,\hat{\phi})\right| < \xi \tag{33}$$

Therefore, the dynamics model of PMLSM can be expressed as

$$\ddot{d} = \phi^{*T}\psi(x) + B_{\mathrm{n}}u + W \tag{34}$$

where $W = D + \xi$ is the total uncertainty, including disturbance, dynamic uncertainty and neural network approximation error. In this process, assume that the total uncertainty is bounded, i.e. $|W| \le \Phi$, Φ is an unknown positive constant. Thus, equation (31) can accurately approximate any value of $f(x)$.

In summary, the overall control law designed is

$$u = B_{\mathrm{n}}^{+}(u_{\mathrm{eq}} + u_{\mathrm{as}}) \tag{35}$$

The equivalent control law is

$$u_{\mathrm{eq}} = -[\hat{\phi}^T\psi(x) + \Pi(e,\varsigma) - \ddot{d}_{\mathrm{m}}] \tag{36}$$

u_{as} is an adaptive control switching law that replaces u_{s} in equation (24)

$$u_{\mathrm{as}} = -(\hat{\Phi} + \rho_1)\mathrm{sign}(S) \tag{37}$$

And the corresponding adaptive update law

$$\dot{\hat{\Phi}} = \frac{1}{\gamma}|S| \tag{38}$$

$$\dot{\hat{\phi}} = \frac{1}{w}S\psi(x) \tag{39}$$

where $\hat{\Phi}$ is the estimated value of the parameter Φ and γ, w are the adaptive gains.

The definition of adaptive estimation error and neural network weight approximation error are respectively

$$\tilde{\Phi} = \hat{\Phi} - \Phi \tag{40}$$

$$\tilde{\phi} = \phi^* - \hat{\phi} \tag{41}$$

Equation (20) is rewritten as

$$\dot{S} = \phi^*\psi(x) + B_{\mathrm{n}}u + W - \ddot{d}_{\mathrm{m}} + \Pi(e,\varsigma) \tag{42}$$

Substituting equations (35)-(37) into equation (42)

$$\dot{S} = \tilde{\phi}^T\psi(x) - (\hat{\Phi} + \rho_1)\mathrm{sign}(S) + W \tag{43}$$

Construct the Lyapunov function:

$$V_2 = \frac{1}{2}S^2 + \frac{\gamma}{2}\tilde{\Phi}^2 + \frac{w}{2}\tilde{\phi}^2 \tag{44}$$

Combining equation (43), the time derivative of V_2 is derived as

$$\begin{aligned}\dot{V}_2 &= S\dot{S} + \gamma\tilde{\Phi}\dot{\tilde{\Phi}} - w\tilde{\phi}\dot{\hat{\phi}}\\ &= S[\hat{\phi}\psi(x) - (\hat{\Phi}+\rho_1)\mathrm{sign}(S) + W] + \gamma(\hat{\Phi}-\Phi)\dot{\hat{\Phi}} - w\tilde{\phi}\dot{\hat{\phi}}\\ &= S\tilde{\phi}\psi(x) - \hat{\Phi}|S| - \rho_1|S| + WS + \gamma(\hat{\Phi}-\Phi)\dot{\hat{\Phi}} - w\tilde{\phi}\dot{\hat{\phi}}\end{aligned} \tag{45}$$

Substituting equations (35)-(37) into equation (45)

$$\begin{aligned}\dot{V}_2 &= -\hat{\Phi}|S| - \rho_1|S| + \Phi S + (\hat{\Phi} - \Phi)|S|\\ &= -\rho_1|S| + WS - \Phi|S|\\ &\le -\rho_1|S|\end{aligned} \tag{46}$$

Because $\dot{V}_2$ is nonpositive, it follows that V_2 is bounded. Therefore, S is also bounded. By integrating both sides of (46) yields

$$\lim_{t\to\infty}\int_0^t \mathrm{d}V \le \lim_{t\to\infty}\int_0^t -\rho_1|S|\mathrm{d}\tau \tag{47}$$

Then

$$\lim_{t\to\infty}\int_0^t \rho_1|S|\mathrm{d}\tau \le \lim_{t\to\infty}(V(0) - V(t)) \le V(0) < \infty \tag{48}$$

Since the S is proved to be bounded, it follows from (48) that ρ_1 is bounded away from zero. Invoking the inequality (48), as the $|S|$ function is uniformly continuous, it follows from Barbalat's Lemma [30,31] that $\lim_{t\to\infty} S = 0$, i.e., the asymptotical convergence of the sliding surface S to zero is guaranteed.

Equation (46) is rewritten as

$$\begin{aligned}\dot{V}_2 &= -\hat{\Phi}\,|S| - \rho_1\,|S| + \Phi S + (\hat{\Phi} - \Phi)\,|S| \\ &= -\rho_1\,|S| + WS - \Phi\,|S| \\ &\leq -\rho_1\,|S| \\ &= -\sqrt{2}\rho_1 V_2^{1/2}\end{aligned} \tag{49}$$

It can be seen that (49) has the form $\dot{V}_2 + \sqrt{2}\rho_1 V_2^{1/2} \leq 0$. Therefore, the time to converge from any initial state $S(0) \neq 0$ to the equilibrium state $S(t_s) = 0$ in the sliding mode is given by [31]

$$t_s \leq \frac{S(0)}{\rho_1} \tag{50}$$

This completes the proof.

IV. EXPERIMENTAL ANALYSIS

In order to prove the effectiveness of the proposed control strategy, the strategy is applied to the position tracking control of PMLSM, and its tracking performance is compared with the tracking performance of NFTSMC. The positional accuracy, response speed and chattering of the control input are compared experimentally.

The structure of the PMLSM control system based on DSP is shown in Fig. 6. The DSP of TMS320F28335 is selected as the core control unit, and the main circuit composed of rectifier and IPM is used as the power supply circuit of PMLSM. The current sensor and the linear grating scale act as detection circuits, and transmit the detected signals to the DSP for real-time monitoring and processing. Once the system fails, the DSP immediately generates a fault protection signal for processing. Fig. 7 is experimental device diagram of PMLSM control system based on DSP. The experimental data is transmitted to the host computer through the 485 serial port.

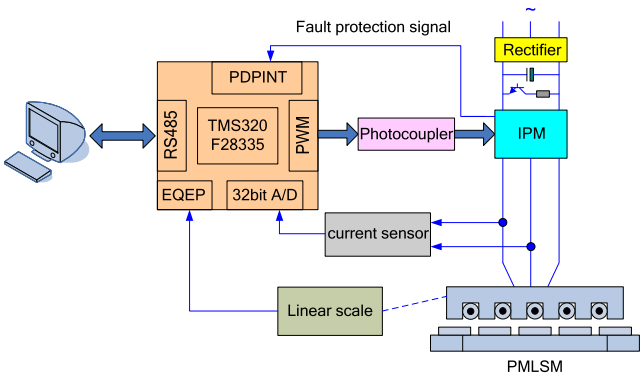

FIGURE 6. Structure diagram of PMLSM control system based on DSP.

The specific parameters of the PMLSM for the experiment are shown in Table 1. In the experiment, the system parameters are debugged several times to obtain the optimal control performance. The parameters are shown in Table 2. The number of three-layer neurons is 2, 5, and 1, respectively.

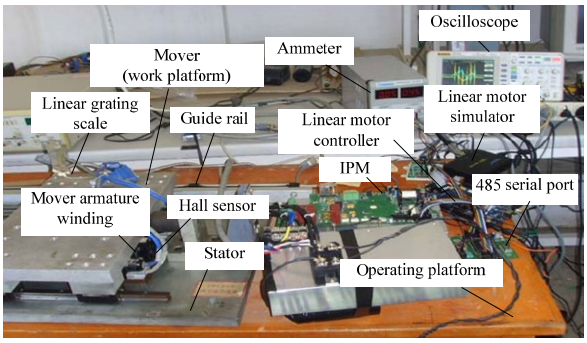

FIGURE 7. Experimental device diagram of PMLSM control system based on DSP.

TABLE 1. Specific parameter values of the PMLSM.

Symbol	PMLSM
M	16.4 kg
B	8 N*s/m
K	50.7 N/A
R	2.1 Ω
τ	32 mm
L_{d}	41.4 mH
L_{q}	41.4 mH
Ψ_{f}	0.09 Wb

TABLE 2. Control Parameters of two methods.

Symbol	NFTSMC	ANNNFTSMC
Γ_1	3	3
Γ_2	300	300
Γ_3	2	2
h_1	0.065	0.065
h_2	40	40
θ	0.5	0.5
α	1.1	1.1
Ω	2	×
ω	×	0.1
ρ_1	3	3
γ	×	0.5
c_i	×	[-1 −0.5 0 0.5 1]
b_i	×	0.5

Experimental studies are carried out on the PMLSM control system using NFTSMC and ANNNFTSMC to verify the effectiveness of the proposed ANNNFTSMC scheme. First, the system is tested with three different signals for experimentation: (i) a step signal with an amplitude of 1 mm, and a sudden load disturbance to the system at 0.5 s; (ii) a sinusoidal signal with an amplitude of 1 mm and a period of 2π s; (iii) a trapezoidal signal with an amplitude of 1 mm.

Then, the tracking and robustness of the PMLSM control system is verified by systematic experiments.

Under the step signal, the variable disturbance curve of the system is shown in Fig. 8. The maximum value of the added disturbance is 50N. The system position tracking curves using two control methods is shown in Fig. 9. At the moment of motor starts, the NFTSMC method reaches a given position at approximately 0.15 s, while the ANNNFTSMC method reaches a given position at approximately 0.1 s and the response speed is faster. After 0.4 s, although there is varying external disturbance, the position tracking curve using the ANNNFTSMC method can still track the given position curve very well. The position tracking curve is not affected by sudden and increasing load disturbance from 0.5 s to 1 s. On this basis, the load disturbance is continuously increased to 50 N from 1 s to 1.5 s, the position tracking curve can still maintain good tracking performance, and the chattering phenomenon is also improved. At the same time, the tracking performance and robust performance of the NFTSMC method decrease under the condition of variable disturbance. Fig. 10 shows the position error curves, the NFTSMC method significantly increases the tracking error at three time points when the system becomes perturbed. The maximum error is about 20 μm. The error of the ANNNFTSMC method is always stable around 5 μm, and the tracking performance is better.

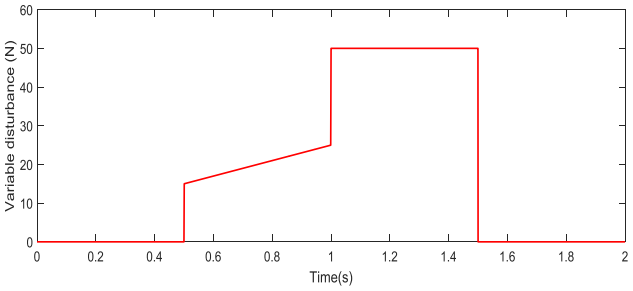

FIGURE 8. Variable disturbance curve for step input.

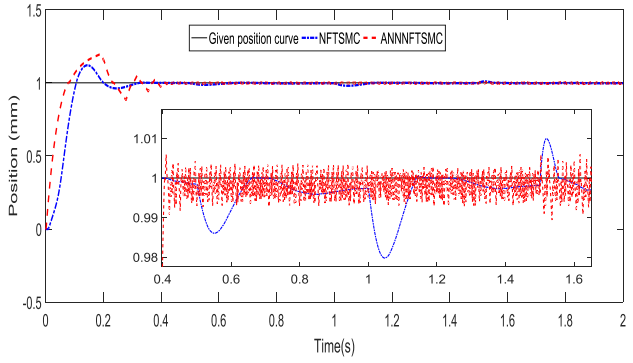

FIGURE 9. Position tracking curves for step input.

Fig. 11 and Fig. 12 are the electromagnetic thrust curve of NFTSMC and their partial amplification respectively. It can be seen from Fig. 11 that the electromagnetic thrust reaches about 250 N at the startup moment of the motor, and then quickly reaches a steady state. Before 0.5 s undisturbed, the peaks occasionally fluctuate and maintain a dynamic balance. After 0.5 s is added to the disturbance, the electromagnetic thrust is continuously adjusted under the action of the controller, and the peak is constantly fluctuating up and down in order to reach the equilibrium state quickly. It can be seen more clearly from Fig. 12 that as the disturbance changes, the electromagnetic thrust is constantly changing towards dynamic equilibrium. After 0.15 s, the load disturbance is reduced to zero, and the electromagnetic thrust also converges toward zero, but the interval of peak fluctuation is too large, which will cause the tracking accuracy of the system to decrease. Fig. 13 is the moving velocity curve. At the moment of starting, the velocity reaches a maximum value of about 0.03 m/s, and then the velocity begins to converge toward equilibrium and finally stabilizes at $\pm$ 0.05 m/s. Fig. 14 and Fig. 15 are the electromagnetic thrust curve and the moving

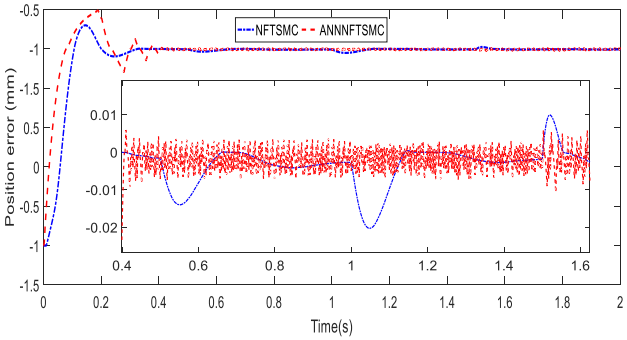

FIGURE 10. Position error curves for step input.

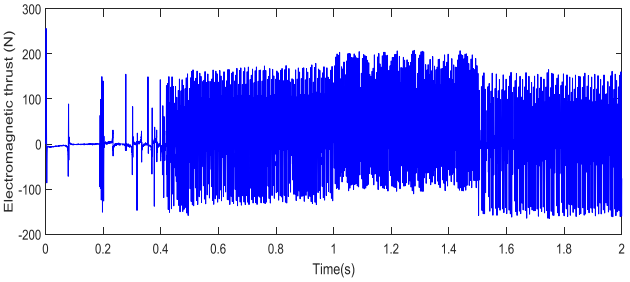

FIGURE 11. NFTSMC electromagnetic thrust curve for step input.

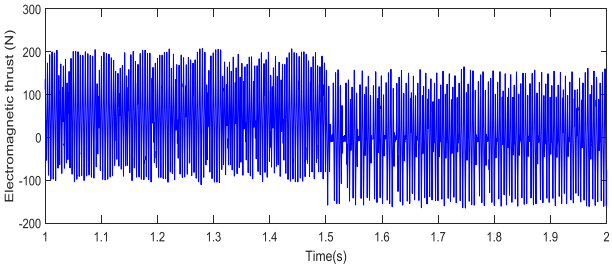

FIGURE 12. Partial amplification curve of electromagnetic thrust for step input.

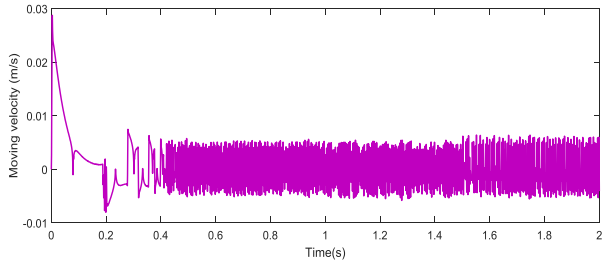

FIGURE 13. NFTSMC moving velocity curve for step input.

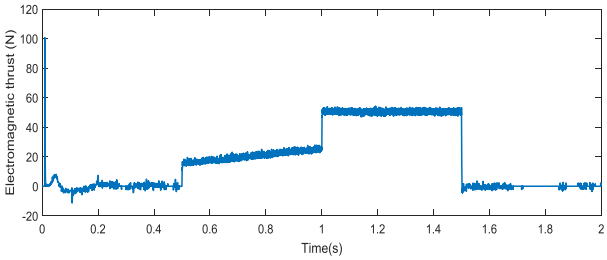

FIGURE 14. ANNNFTSMC electromagnetic thrust curve for step input.

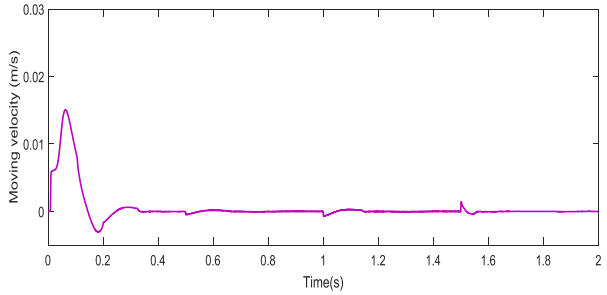

FIGURE 15. ANNNFTSMC moving velocity curve for step input.

velocity curve of the ANNNFTSMC, respectively. It can be seen from Fig. 14 that the electromagnetic thrust reaches about 100 N at the moment when the motor starts up, then starts to decrease and quickly reaches the equilibrium state, and the system remains in a stable state no matter how the disturbance change. Therefore, when a variable disturbance occurs at 0.5 s, the electromagnetic thrust is basically equal to the variable disturance. In Fig. 15, the maximum value of the starting moment moving velocity reaches 0.015 m/s, and then rapidly decreases toward the equilibrium state. After 0.2 s, no matter how the external disturbance changes, the moving velocity is always near the equilibrium state and the fluctuation is extremely small, so that the system has higher position tracking accuracy. In summary, ANNNFTSMC can attenuate chattering and improve the tracking and robustness of the servo system.

Under the sinusoidal signal, the position tracking curves of the two control methods is shown in Fig. 16. The tracking curve of NFTSMC fluctuates near the curve of the given position, and there is a serious chattering phenomenon. The ANNNFTSMC can track the given position curve very well. The chattering phenomenon is obviously improved.

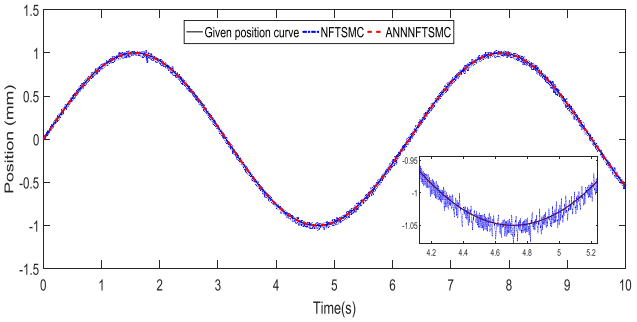

FIGURE 16. Position tracking curves for sinusoidal input.

Fig. 17 shows the position error curve of NFTSMC. The maximum error of the system can reach 5.9 μm, and the chattering phenomenon is serious. Fig. 18 shows the position error curve of ANNNFTSMC. At the moment of motor starts, the error can quickly converge to near zero, and finally stabilize at around 0.5 μm. The tracking error is small and the chattering is weakened. Compared with NFTSMC, it shows that the adaptive RBF neural network can obtain accurate PMLSM dynamic mathematical model by approximation and can estimate the upper bound of total uncertainty in real time online, and improve the tracking accuracy of the system. In summary, the ANNNFTSMC method not only has higher tracking accuracy and faster response speed, but also improves the chattering phenomenon.

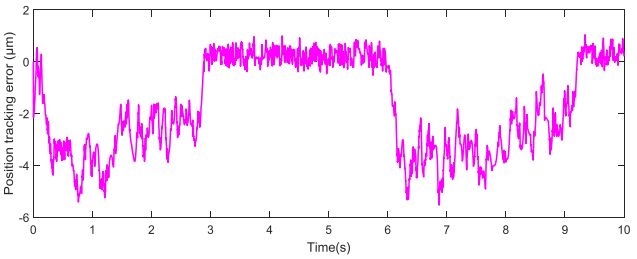

FIGURE 17. NFTSMC position error curve for sinusoidal input.

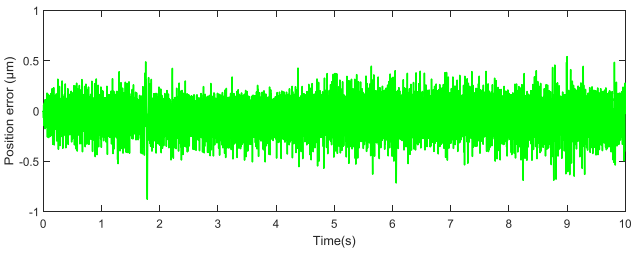

FIGURE 18. ANNNFTSMC position error curve for sinusoidal input.

To evaluate the output performance, calculate the mean square error (MSE) of the tracking position. The total sampling time is T, the expected position is d_{m} and the actual position is d, and the tracking position mean square error (MSE) is given in equation (51).

$$MSE = \frac{1}{T}\sum_{t=1}^{T}(d_{\mathrm{m}} - d)^2 \tag{51}$$

The average values of the MSE for position tracking under the two control methods are given in Table 3. As can be seen from the table, ANNNFTSMC provides a minimum MSE value compared to NFTSMC (i.e., the ANNNFTSMC system has better tracking performance). The position tracking MSE response curves of the two control methods is shown in Fig. 19. The MSE of ANNNFTSMC is much smaller than NFTSMC and is basically stable near zero, so the tracking effect of ANNNFTSMC is better.

TABLE 3. MSE examination of NFTSMC and ANNNFTSMC.

Method / Value	NFTSMC	ANNNFTSMC
MSE	4.174e-11	4.941e-13

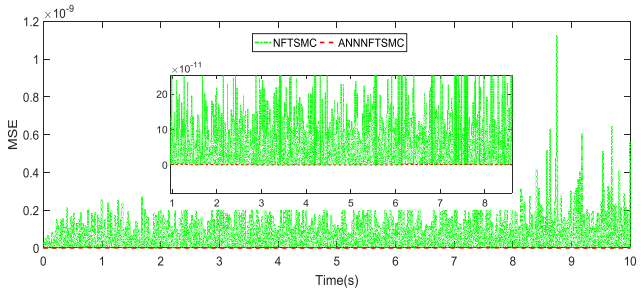

FIGURE 19. MSE response curves for position tracking.

In order to better reflect the credibility of the tracking error, a relative error is introduced. Relative error refers to the value obtained by multiplying the ratio of the absolute error caused by the measurement to the measured true value by 100%, expressed as a percentage, which is a dimensionless value. The relative error δ of position tracking is given in equation (52), and the relative error curve is given as shown in Figure 20.

$$\delta = \frac{|d - d_{\mathrm{m}}|}{d_{\mathrm{m}}} \times 100\% = \frac{|e|}{d_{\mathrm{m}}} \times 100\% \tag{52}$$

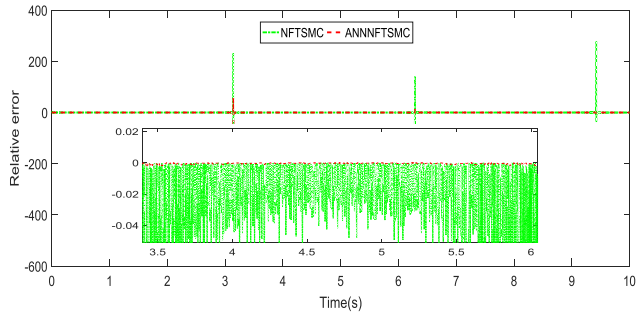

FIGURE 20. Relative error curves for two control methods.

It can be seen from the Fig. 20 that the relative error curves under the two control methods are all near zero, and the discrimination effect is not obvious. In order to better compare the advantages and disadvantages of the two control methods, a section of the curves is amplified. The relative error curve of ANNNFTSMC converges to near zero and has no fluctuation. It is obvious that the relative error curve of NFTSMC is severely fluctuating and the convergence effect is poor. It can be seen that the position tracking performance of ANNNFTSMC is better than that of NFTSMC.

Under the trapezoidal signal, the position tracking curves of the two control methods are shown in Fig. 21. Both NFTSMC and ANNNFTSMC can track the given position curve well. The tracking effect of ANNNFTSMC is obviously better than that of NFTSMC, and the chattering phenomenon is obviously improved. Fig. 22 is the position tracking error curves under two control methods. It can be seen from the figure that the position error of NFTSMC is larger than that of ANNNFTSMC. The position error range is between -0.07-0.05mm, and the maximum can reach 0.07mm. The chattering phenomenon is more serious, and the position error of ANNNFTSMC is smaller, basically stable near zero, and the tracking performance of the system is better. In order to better compare the experimental results, the position error curve of ANNNFTSMC is shown in Fig. 23. The position error range is -0.01-0.005mm, and the error is much smaller than the position error of NFTSMC.

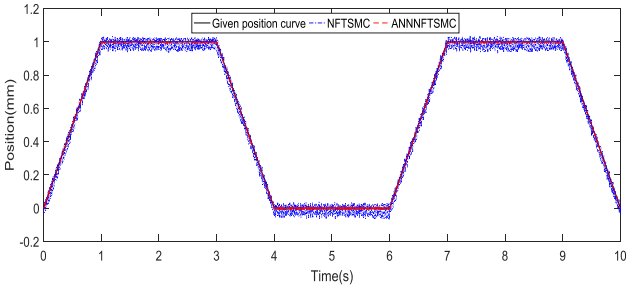

FIGURE 21. Position tracking curves for trapezoidal input.

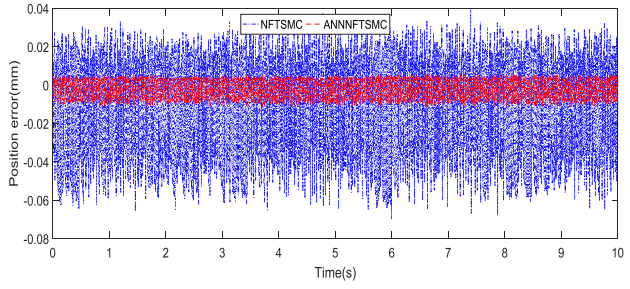

FIGURE 22. Position error curves for trapezoidal input.

In order to more comprehensively evaluate the control performance of the two methods, ANNNFTSMC and NFTSMC, the tracking position mean square error (MSE) and relative error curves of the two control methods are given below.

The average of the position tracking MSE under the NFTSMC and ANNNFTSMC methods is given in Table 4.

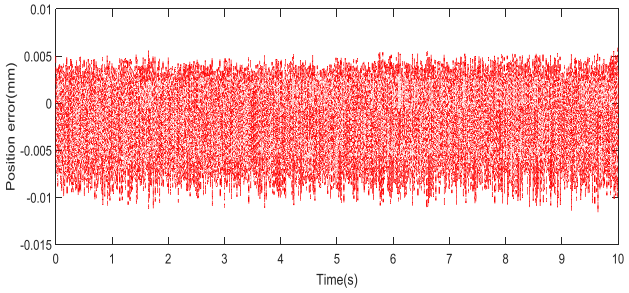

FIGURE 23. ANNNFTSMC position error curve for trapezoidal input.

TABLE 4. MSE examination of NFTSMC and ANNNFTSMC.

Method / Value	NFTSMC	ANNNFTSMC
MSE	6.745e-11	1.886e-12

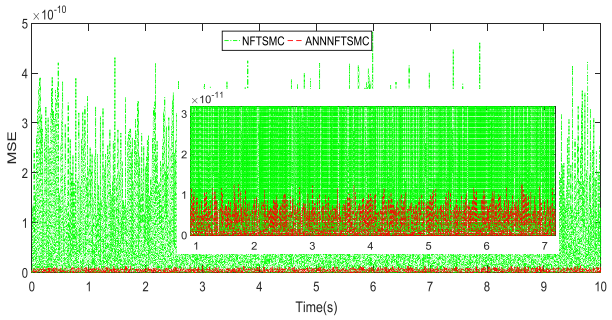

FIGURE 24. MSE response curves for position tracking.

The MSE average of the ANNNFTSMC is 1.86e-12, which is much smaller than the average of 6.74e-11 of the NFTSMC. Therefore, the ANNNFTSMC system has better tracking performance. The position tracking MSE response curves of the two control methods is shown in Fig. 24. Macroscopically, the MSE value of NFTSMC is much larger than the MSE value of ANNNFTSMC, and its maximum MSE value can reach 4.7e-10. Microscopically, the maximum MSE value of ANNNFTSMC is 1.3e-11. Therefore, the system using the ANNNFTSMC method has better output performance.

Fig. 25 is the relative error curves of the two control methods. It can be seen from the figure that the relative error of NFTSMC is significantly larger than the relative error of ANNNFTSMC. The relative error of NFTSMC is basically stable at around 1%, while the relative error of ANNNFTSMC is basically stable near zero, and the tracking performance is far superior to NFTSMC.

The position tracking error of the two control methods of NFTSMC and ANNNFTSC under three different input signals is summarized in Table 5.

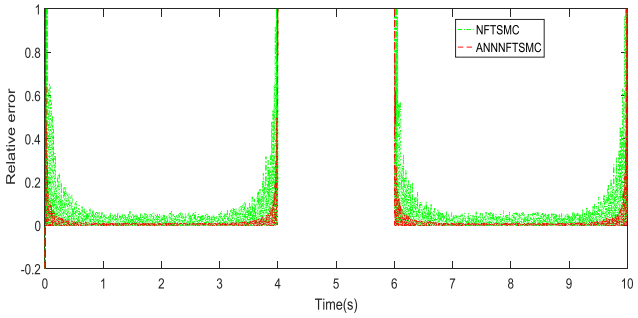

FIGURE 25. Relative error curves for two control methods.

TABLE 5. Position tracking error under different inputs.

Input / Error	Step signal	Sinusoidal signal	Trapezoidal signal
NFTSMC	-0.02-0.01mm	-5.8-1μm	-0.07-0.03mm
ANNNFTSMC	-0.01-0.005mm	-0.7-0.5μm	-0.011-0.005mm

V. CONCLUSION

In view of the uncertainties such as parameter variation and load disturbance in the PMLSM servo system, two control schemes, NFTSMC and ANNNFTSMC, are designed. Based on NFTSMC, an adaptive RBF neural network is used to approximate the unknown part function in PMLSM modeling without an accurate dynamic model. By comparing and analyzing the experimental results of the two control schemes, it is found that ANNNFTSMC not only inherits the advantages of NFTSMC, such as nonsingularity, finite time convergence, fast transient response, small steady-state error and high position tracking accuracy, but also weakens chattering and has stronger robustness.

ACKNOWLEDGMENT

The authors would like to thank the associate and reviewer for the constructive comments and suggestions that have helped improved the quality and presentation of this paper.

REFERENCES

[1] M.-Y. Chen and J.-S. Lu, "High-precision motion control for a linear permanent magnet iron core synchronous motor drive in position platform," *IEEE Trans Ind. Informat.*, vol. 10, no. 1, pp. 99–108, Feb. 2014.

[2] X. M. Zhao and J. W. Zhao, "Intelligent complementary sliding mode control for permanent magnet linear synchronous motor," *Trans. Chin. Electrotech. Soc.*, vol. 31, no. 23, pp. 9–14, Dec. 2016.

[3] X. M. Zhao and C. G. Wang, "Adaptive incremental sliding mode control for permanent magnet linear synchronous motor," *Trans. Chin. Electrotech. Soc.*, vol. 32, no. 11, pp. 111–117, Jun. 2017.

[4] T. L. Le, "Intelligent fuzzy controller design for Antilock braking systems," *J. Intell. Fuzzy Syst.*, vol. 36, no. 4, pp. 3303–3315, 2019.

[5] J. Chen, C. Xu, C. Wu, and W. Xu, "Adaptive fuzzy logic control of fuel-cell-battery hybrid systems for electric vehicles," *IEEE Trans. Ind. Informat.*, vol. 14, no. 1, pp. 292–300, Jan. 2018.

[6] M. Sharma and S. P. Singh, "Fuzzy sliding mode control of plate vibrations," *Shock Vib.*, vol. 17, no. 1, pp. 71–92, 2010.
[7] Y. K. Wu and X. M. Zhao, "Adaptive backstepping control based on functional link radial basis function neural network for PMLSM," *Trans. Chin. Electrotech. Soc.*, vol. 33, no. 17, pp. 4044–4051, Sep. 2018.
[8] B. Oh, J. Jeong, J. Suk, and S. Kim, "Design of a control system for an organic flight array based on a neural network controller," *Int. J. Aerosp. Eng.*, vol. 2018, pp. 1–11, Jul. 2018.
[9] F. Luan, J. Na, Y. Huang, and G. Gao, "Adaptive neural network control for robotic manipulators with guaranteed finite-time convergence," *Neurocomputing*, to be published, doi: 10.1016/J.NEUCOM.2019.01.063.
[10] G. Navarro-Guerrero and Y. Tang, "Fractional order model reference adaptive control for anesthesia," *Int. J. Adapt. Control Signal Process.*, vol. 30, no. 9, pp. 1350–1360, Feb. 2017.
[11] T. R. Oliveira, V. H. P. Rodrigues, and L. Fridman, "Generalized model reference adaptive control by means of global HOSM differentiators," *IEEE Trans. Autom. Control*, vol. 64, no. 5, pp. 2053–2060, May 2019.
[12] G. Song and G. Tao, "Adaptive state-feedback control with sensor failure compensation for asymptotic output tracking," *Int. J. Adapt. Control Signal Process.*, vol. 33, no. 1, pp. 130–156, Nov. 2019.
[13] S. Eshghi and R. Varatharajoo, "Nonsingular terminal sliding mode control technique for attitude tracking problem of a small satellite with combined energy and attitude control system (CEACS)," *Aerosp. Sci. Technol.*, vol. 76, pp. 14–26, May 2018.
[14] S. Kamal, J. Moreno, and A. Chalanga, "continuous terminal sliding-mode controller," *Automatica*, vol. 69, pp. 308–314, 2016.
[15] S. J. Gambhire, K. S. S. Kanth, and G. M. Malvatkar, "Robust fast finite-time sliding mode control for industrial robot manipulators," *Int. J. Dynam. Contr.*, vol. 7, no. 2, pp. 607–618, Sep. 2018.
[16] H. Yuan and X. M. Zhao, "Direct thrust force control based on integral sliding mode for permanent magnet linear synchronous motor," *Trans. Chin. Electrotech. Soc.*, vol. 34, no. 3, pp. 483–488, Feb. 2019.
[17] T. Madani, B. Daachi, and K. Djouani, "Modular-controller-design-based fast terminal sliding mode for articulated exoskeleton systems," *IEEE Trans. Control Syst. Technol.*, vol. 25, no. 3, pp. 1133–1140, May 2017.
[18] A. Safa, R. Y. Abdolmalaki, S. Shafiee, and B. Sadeghi, "Adaptive nonsingular terminal sliding mode controller for micro/nanopositioning systems driven by linear piezoelectric ceramic motors," *ISA Trans.*, vol. 77, pp. 122–132, Jun. 2018.
[19] X. M. Zhao and Y. K. Wu, "Backstepping control based on adaptive modified Laguerre Recurrent neural network for permanent magnet linear synchronous motor," *Trans. Chin. Electrotech. Soc.*, vol. 33, no. 10, pp. 230–237, May 2018.
[20] H. B. Zhao and C. G. Wang, "Radial-basis-function neural network backstepping adaptive control of dual-motor driving servo system," *Contr. Theory Appl.*, vol. 35, no. 9, pp. 60–72, Sep. 2018.
[21] G. Chen, B. Jin, and Y. Chen, "Nonsingular fast terminal sliding mode posture control for six-legged walking robots with redundant actuation," *Mechatronics*, vol. 50, pp. 1–15, Apr. 2018.
[22] L. Qiao and W. D. Zhang, "Trajectory tracking control of AUVs via adaptive fast nonsingular integral terminal sliding mode control," *IEEE Trans. Ind. Informat.*, to be published, doi: 10.1109/TII.2019.2949007.
[23] L. Qiao and W. Zhang, "Adaptive second-order fast nonsingular terminal sliding mode tracking control for fully actuated autonomous underwater vehicles," *IEEE J. Ocean. Eng.*, vol. 44, no. 2, pp. 363–385, Apr. 2019.
[24] Y. Wang, F. Yan, and J. W. Chen, "A new adaptive time-delay control scheme for cable-driven manipulators," *IEEE Trans. Ind. Informat.*, vol. 15, no. 6, pp. 3469–3481, Oct. 2018, doi: 10.1109/TII.2018.2876605.
[25] Y. Wang, L. Gu, Y. Xu, and X. Cao, "Practical tracking control of robot manipulators with continuous fractional-order nonsingular terminal sliding mode," *IEEE Trans. Ind. Electron.*, vol. 63, no. 10, pp. 6194–6204, Oct. 2016.
[26] Y. Wang, K. W. Zhu, B. Chen, and M. L. Jin, "Model-free continuous nonsingular fast terminal sliding mode control for cable-driven manipulators," *ISA Trans.*, to be published, doi: 10.1016/J.ISATRA.2019.08.046.
[27] Q. D. Guo, C. Y. Wang, and M. W. Zhou, *Precision Control Technology for Linear AC Servo System*. Beijing, China: Mechanical Industry Press, 2000.
[28] L. Qiao and W. Zhang, "Double-loop integral terminal sliding mode tracking control for UUVs with adaptive dynamic compensation of uncertainties and disturbances," *IEEE J. Ocean. Eng.*, vol. 44, no. 1, pp. 29–53, Jan. 2019.
[29] Z. Wu, Y. Xia, and X. Xie, "Stochastic Barbalat's lemma and its applications," *IEEE Trans. Autom. Control*, vol. 57, no. 6, pp. 1537–1543, Jun. 2012.
[30] Department of Mathematics, East China Normal University, *Mathematical Analysis*, vol. 1, 4th ed. Beijing, China: Higher Education Press, 2010, pp. 4–7.
[31] S. P. Bhat and D. S. Bernstein, "Finite-time stability of continuous autonomous systems," *SIAM J. Control Optim.*, vol. 38, no. 3, pp. 751–766, Jan. 2000.

XIMEI ZHAO was born in Changchun, Jilin, China, in 1979. She received the B.S., M.S., and Ph.D. degrees in electrical engineering from the Shenyang University of Technology, Shenyang, China, in 2003, 2006, and 2009, respectively. She is currently a Professor and the Ph.D. Supervisor with the School of Electrical Engineering, Shenyang University of Technology. She has authored or coauthored more than 100 technical articles, three textbooks, and holds 15 patents in these areas. Her research interests are electrical machines, motor drives, motor control, intelligent control and robot control.

DONGXUE FU received the B.S. degree in electrical engineering and automation from Beihua University, Jilin, China, in 2017. He is currently pursuing the Ph.D. degree with the School of Electrical Engineering, Shenyang University of Technology. His current research interests include motor control, intelligent control, and neural networks.